XFlowMP: Task-Conditioned Motion Fields for Generative Robot Planning with Schrödinger Bridges

Khang Nguyen¹ and Minh Nhat Vu^{2,3}

Abstract—Generative robotic motion planning requires not only the synthesis of smooth and collision-free trajectories but also feasibility across diverse tasks and dynamic constraints. Prior planning methods, both traditional and generative, often struggle to incorporate high-level semantics with low-level constraints, especially the nexus between task configurations and motion controllability. In this work, we present XFlowMP, a task-conditioned generative motion planner that models robot trajectory evolution as entropic flows bridging stochastic noises and expert demonstrations via Schrödinger bridges given the inquiry task configuration. In specific, our method leverages Schrödinger bridges as a conditional flow matching coupled with a score function to learn motion fields with high-order dynamics while encoding start-goal configurations, enabling the generation of collision-free and dynamically-feasible motions. Through evaluations, XFlowMP achieves up to 53.79% lower maximum mean discrepancy, 36.36% smoother motions, and 39.88% lower energy consumption while comparing to the next-best baseline on the RobotPointMass benchmark and also reducing short-horizon planning time by 11.72%. On long-horizon motions in the LASA Handwriting dataset, our method maintains the trajectories with 1.26% lower maximum mean discrepancy, 3.96% smoother, and 31.97% lower energy. We further demonstrate the practicality of our method on the Kinova Gen3 manipulator, executing planning motions and confirming its robustness in real-world settings.

I. Introduction

Task-conditioned motion planning is one of the central problems in robot planning, entailing the systems to generate trajectories that satisfy specific constraints defined by the task at hand. Traditional approaches often rely on optimizationbased methods, including sampling-based planners [1], graph search algorithms [2], and trajectory optimization techniques [3], [4]. As task requirements are encoded through cost functions that find optimal paths through search or iterative refinement, such approaches often struggle with scalability, adaptability, and generalization to diverse, complex tasks [5], [6]. Moreover, these methods are computationally expensive when computing trajectories from scratch and heavily rely on good initialization. In the meantime, generative motion planning offers an alternative approach that directly learns the distribution of expert trajectories from data, enabling the fast sampling of diverse, context-adaptive solutions that naturally balance task semantics with physical feasibility.

Recent advances in generative modeling have introduced a new paradigm for context-conditioned modeling, where

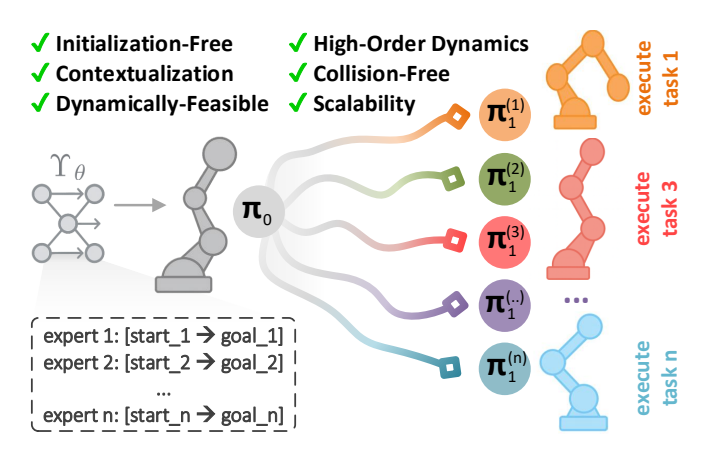


Fig. 1: Overview with XFlowMP: The task-conditioned motion planner, Υ_{θ} , learns from diverse experts to generate trajectories based on task inputs. From an initial noise distribution π_0 , the learned model with Schrödinger bridges is able to produce multiple valid solutions $\pi_1^{(i)}$, while being initialization-free, contextualized, dynamically-feasible, collision-free, and scalable. Thus, the generated trajectories can be executed on robots across a variety of tasks.

output is synthesized directly from data distributions conditioned on input specifications, particularly in protein docking [7], [8], image generation [9], [10], language-driven planning [11], and text-to-speech generation [12]. Within this realm, generative-based approaches have leveraged foundational probabilistic models, such as conditional variational autoencoders [13], [14], normalizing flows [15], [16], and diffusion [17], [18], to learn mappings from inputs (*e.g.*, prompts) to image distributions. By conditioning image synthesis on contextual inputs, these models can flexibly generate new samples and produce diverse outputs that satisfy specified semantic or structural constraints, moving beyond the limitations of traditional optimization-based techniques [19], [20].

Extending these conditional generative models to motion planning requires producing temporally coherent trajectories that satisfy dynamic, physical, and task-specific constraints [21], [22]. Leveraging task contexts as semantic inputs, such as start and goal states, enables the generation of trajectories that are not only feasible and collision-free but also adaptive and diverse across various scenarios. As trajectories are high-dimensional and continuous, it also requires such models to capture long-range temporal dependencies while maintaining smoothness and feasibility [23], [24]. In addition, diverse tasks and environments demand robust generalization, often from limited demonstrations [25], [26]. Moreover, the problem of complying with physical constraints such as kinematics, dynamics, and collision avoidance is typically challenging to encode in generative motion planners.

¹Mohamed bin Zayed University of Artificial Intelligence (MBZUAI), Abu Dhabi, UAE

²Automation & Control Institute (ACIN), TU Wien, Vienna, Austria

³Austrian Institute of Technology (AIT) GmbH, Vienna, Austria

[†]Corresponding authors / e-mails: khang.nguyen@mbzuai.ac.ae, minh.vu@tuwien.ac.at

In general, the central problem lies in modeling trajectories that are simultaneously high-dimensional, high-order dynamics, and sequential in nature, which makes capturing long-range dependencies while ensuring smoothness and feasibility particularly challenging. These difficulties are compounded by the need to integrate physical and environmental constraints, such as collision avoidance and kinematic limits. While recent advances in conditional trajectory generation have made progress [21], [27], scalable and reliable solutions that address these intertwined challenges in a unified generative framework remain an open research problem.

To address these limitations, we propose Schrödinger Flow Motion Planning, namely XFlowMP, a task-conditioned generative framework (Fig. 1) that models high-dimensional robot motions as entropic flows evolving from noises to expert demonstrations. In specific, XFlowMP leverages motion fields with learnable score-based functions to generate smooth, dynamically-feasible, and collision-free trajectories with high-order dynamics while respecting start-goal configurations and dynamic constraints. By unifying positional, velocity, and acceleration fields with Schrödinger bridges, our method implicitly encodes high-order dynamics and preserves the scalability of trajectories. Meanwhile, the score function guides the conditional generation in the latent space, guaranteeing a tight distributional alignment with expert demonstrations. Our contributions are stated as follows:

- 1) We devise a initialization-free, task-conditioned generative motion planner using Schrödinger bridges.
- We unify task-conditioned motion fields with velocity, acceleration, and jerk fields for the generation of scalable, dynamically-feasible, and collision-free motions.
- 3) We validate the performance of our proposed method on RobotPointMass and LASA Handwriting datasets for comprehensive evaluations and through real-world experiments on a real-robot system.

II. RELATED WORK

Optimal Transport for Motion Field Synthesis: Optimal transport (OT) has been shown as a strong framework for generative modeling, with most prior works applying OT, Schrödinger bridges [28] and diffusion models [16], [17], [29] to the field of image generation [9], [10] and cell synthesis [7], [8]. Recent advances have extended OT-based generative models to video synthesis [30] and 3D shape generation [31], demonstrating the versatility of OT in highdimensional domains. Building on these foundations, OTbased approaches have begun to address motion planning and trajectory generation in cellular synthesis, including trajectory interpolation [23], [32]. In robotics, conditional generative models [21], [33] and neural ordinary differential equations (ODEs) [24], [34] further enhance the flexibility and robustness of motion synthesis, enabling context-aware trajectory generation. To bridge the gap between image generation and trajectory synthesis, our approach seeks the derivation task-conditioned motion fields for generative motion robotic planning by implicitly contextualizing tasks and applying Schrödinger bridge-based flow matching.

Task-Conditioned Generative Planning: The field of generative modeling has witnessed a paradigm shift driven by advances in conditional synthesis [20], [35]. Prior works in text-to-image and text-to-video [36], [37] have demonstrated the remarkable ability to generate high-fidelity, diverse outputs conditioned on rich semantic prompts, enabling users to specify complex visual and temporal content through natural language [38]. While these generative models offer powerful semantic conditioning, directly applying them to robotics presents significant challenges due to the need for precise control, safety, and real-time adaptation in physical environments [39], [40]. Bridging the gap requires integrating domain knowledge, robust perception, and control mechanisms to ensure generated behaviors are feasible, reliable, and interpretable for autonomous robotic systems [25], [26], [41]. Inspired by recent advances, we propose a task-conditioned generative framework for robotic motion planning. By adapting task-driven synthesis and Schrödinger bridge-based flow matching, our method enables robots to generate scalable, collision-free, physically-feasible trajectories with high-order dynamics, which are constrained by the environment.

Robot Planning with Schrödinger Bridges: Schrödinger bridge theory has gained traction as a powerful tool for optimal control and distribution steering in complex robotic systems. Sahoo et al. [42] extend these ideas to the setting of Lie groups, analyzing the behavior of controlled dynamics and providing a geometric perspective on Schrödinger-based control. Later, Bakshi et al. [43] introduce a Schrödinger bridge approach for controlling large populations, demonstrating how stochastic optimal transport can be leveraged for population-level control tasks. Caluya and Halder [44] develop the reflected Schrödinger bridge framework, enabling density control under explicit path constraints, which is particularly relevant for robotics and autonomous systems operating in constrained environments. Eldesoukey and Georgiou [45] further generalize Schrödinger bridge control and estimation to spatio-temporal distributions on graphs, opening new avenues for distributed and networked control. Mirrahimi et al. [46] explore Lyapunov-based control of bilinear Schrödinger equations, providing theoretical guarantees for stability and convergence in quantum and classical systems. To push these theoretical solutions for robot planning more scalable and in a practical manner, our approach looks into the coupling between neural ODEs and score functions as learnable components for robotic planning, while preserving their high-order dynamics and scalability.

III. SCHRÖDINGER FLOW MOTION PLANNING

A. Problem Formulation

Consider a workspace $\mathcal W$ in which a robot can navigate from a start configuration to a goal configuration while avoiding obstacles and satisfying dynamic constraints. We define the set of N expert demonstration motions as:

$$\mathcal{D} = \left\{ \boldsymbol{\pi}^{(i)} = \left\{ \mathbf{q}_t^{(i)}, \dot{\mathbf{q}}_t^{(i)}, \ddot{\mathbf{q}}_t^{(i)} \right\}_{t=0}^T \;\middle|\; \mathbf{q}_0^{(i)} \in \mathcal{S}, \; \mathbf{q}_T^{(i)} \in \mathcal{G} \right\},$$

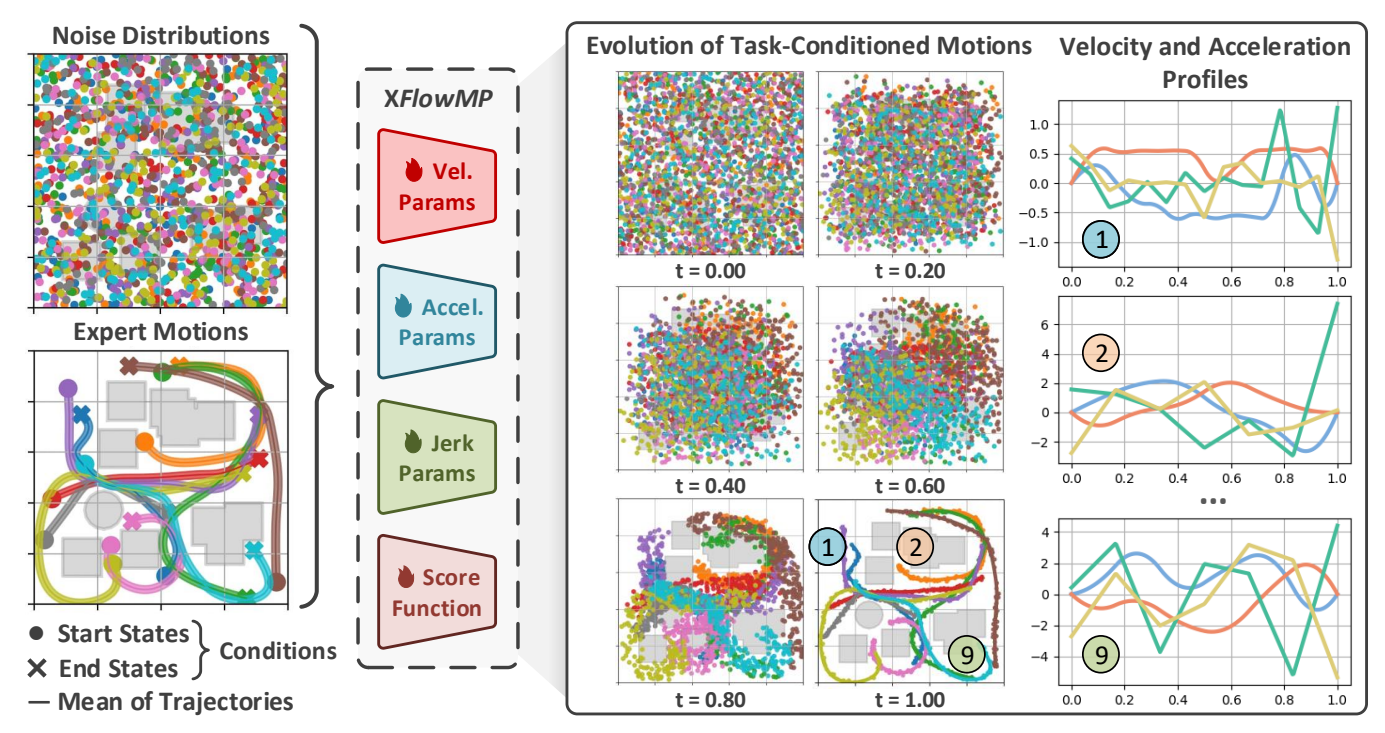


Fig. 2: Methodology of XFlowMP: Given expert demonstrations of motions in the maze environment, XFlowMP contextualizes those motions by their start-goal pairs (\P , \ref{x}) as tasks. During training, the learnable parameters transport initial noise distributions to match expert trajectories through Schrödinger bridges, ensuring that the generated trajectories remain consistent with task inputs. In specific, the motion field, comprising velocity, acceleration, and jerk parameters, learns to generate high-order motions along the evolution horizon from 0 to 1. Meanwhile, the score function estimates the underlying task-dependent gradients that guide the flows toward expert distributions. The corresponding velocity (blue and orange) and acceleration (green and yellow) profiles of the paths are shown accordingly. At t = 1.00, XFlowMP generates motions that are collision-free and dynamically-feasible while maintaining semantic consistency with task conditions.

where $\pi^{(i)}$ denotes the motion for the *i*-th task, $\mathbf{q}_t^{(i)} \in \mathbb{R}^d$ is the robot's state at time step t along the planning horizon from 0 to T, $S \subset \mathcal{W}$ and $\mathcal{G} \subset \mathcal{W}$ denote the sets of start and goal states within the robot workspace, respectively.

To learn the generative model for robotic motion planning, we first define the distributions of expert trajectories as positional states, \mathbf{Q} , and their velocity and acceleration states, $\dot{\mathbf{Q}}$ and $\ddot{\mathbf{Q}}$, respectively. We denote $\pi_0 = \{\varepsilon_{\mathbf{Q}}, \varepsilon_{\dot{\mathbf{Q}}}, \varepsilon_{\ddot{\mathbf{Q}}}\}$ and $\pi_1 = \{\mathbf{Q}, \dot{\mathbf{Q}}, \ddot{\mathbf{Q}}\}$ as the noise and target motion distributions, respectively, and utilize flows to transport from the source distribution π_0 to the target distribution π_1 . Given such an expert dataset \mathcal{D} , our goal thus is to learn a generative planner that can synthesize scalable, collision-free, and dynamically feasible trajectories with high-order dynamics under multiple start-goal configurations within the robot workspace. The neural planner can be formally written as follows:

$$\Upsilon_{\theta}(\mathbf{q}_0, \mathbf{q}_T, \pi_0 \mid \mathcal{D}, \mathcal{W}) \to \pi_1', \text{ with } \mathbf{q}_0 \in \mathcal{S}, \mathbf{q}_T \in \mathcal{G}$$
 (1)

where Υ_{θ} represents the learnable motion field with learnable parameters θ and $\pi_1' = \{\mathbf{q}_t'\}_{t=0}^T \notin \mathcal{D}$ denotes the generated trajectory that is conditioned by the start-goal states $(\mathbf{q}_0, \mathbf{q}_T)$ within the robot workspace \mathcal{W} . From here, we refer to the start-goal states as a task, denoted as \mathcal{T} , for simplicity.

B. Motion Field with Schrödinger Bridges

Given a reference stochastic process \mathbb{Q} with law on motions of π , the Schrödinger bridge finds the motion distribution \mathbb{P}^* closest to \mathbb{Q} via Kullback–Leibler (KL) divergence,

matching the source distribution π_0 to target distribution π_1 :

$$\mathbb{P}^* = \arg \min_{\mathbb{P}: \ \mathbb{P}_0 = \pi_0, \mathbb{P}_1 = \pi_1} \ \mathrm{KL} \left(p_t(\pi) \mid\mid q_t \right), \tag{2}$$

where $p_t(\pi) \in \mathbb{P}$ represents the evolving probability flows and $q_t \in \mathbb{Q}$ is a reference measure of the stochastic process.

From the vanilla motion field Υ of the time-dependent flow ψ_t [27], the stochastic differential equation (SDE) of a motion field under entropic flows $\Upsilon(\psi(\pi))$ is defined as:

$$d\psi_t = \Upsilon_t \left(\psi(\pi) \right) dt + \sigma_t dw_t, \tag{3}$$

where ψ denotes the entropic flows and w models a time-independent Brownian motion with diffusion strength of σ . Also, based on the well-known Fokker-Planck equation [47], [48], the continuity equation is given as:

$$\frac{dp(\pi)}{dt} = -\nabla \cdot \left[p_t(\pi) \Upsilon_t \left(\psi(\pi) \right) \right] + \frac{1}{2} \sigma_t^2 \Delta p_t(\pi), \quad (4)$$

where the advection term describes the transport of probability mass and the diffusion term models the spreading effect of noise. Thus, to obtain an ODE that preserves the same marginal distributions $p_t(\pi)$ in Eq. 4, we rewrite the probability flow ODE from its SDE in Eq. 3:

$$\Upsilon_t'(\psi(\pi)) = \Upsilon_t(\psi(\pi)) - \frac{1}{2}\sigma_t^2 \nabla \log p_t(\pi), \qquad (5)$$

where $\Upsilon_t'(\psi(\pi))$ is the equivalent drift function that ensures that $p_t(\pi)$ evolves as in Eq. 4, and $\nabla \log p_t(\pi)$ is the score function. Under the linear-Gaussian reference processes in

Algorithm 1: Schrödinger Flow Motion Planning

Input : $\pi_1 = {\mathbf{Q}, \dot{\mathbf{Q}}, \ddot{\mathbf{Q}}} := \text{expert motions},$ $\pi_0 = \{ \varepsilon_{\mathbf{Q}}, \varepsilon_{\dot{\mathbf{Q}}}, \varepsilon_{\ddot{\mathbf{Q}}} \} \coloneqq \text{noise distributions},$ $\sigma := \text{diffusion strength}, \ \lambda(t) := \text{scheduler}$ **Output:** $\Upsilon_{\theta} := \text{motion field}, g_{\theta} := \text{score function}$ 1 **function** train_xflowmp $(\pi_1, \pi_0, \sigma, \lambda(t))$ while training do 2 Sample $t \sim \mathcal{U}[0, 1]$ 3 Sample expert minibatch $(\mathbf{q}_1, \dot{\mathbf{q}}_1, \ddot{\mathbf{q}}_1) \sim \pi_1$ 4 5 Sample noise minibatch $(\varepsilon_{\mathbf{q}}, \varepsilon_{\dot{\mathbf{q}}}, \varepsilon_{\dot{\mathbf{q}}}) \sim \pi_0$ $\mathcal{T} \leftarrow \text{get_start_goal_states}(\mathbf{q}_1)$ 6 $\mathbf{q}_t \leftarrow \text{interp}(\mathbf{q}_1, \varepsilon_{\mathbf{q}}, \varepsilon_{\dot{\mathbf{q}}}, \varepsilon_{\ddot{\mathbf{q}}}, t) \text{ (Eq. 10)}$ 7 $\Upsilon_t \leftarrow \text{get_fields}(\mathbf{q}_1, \dot{\mathbf{q}}_1, \ddot{\mathbf{q}}_1, \varepsilon_{\mathbf{q}}, \varepsilon_{\dot{\mathbf{q}}}, \varepsilon_{\ddot{\mathbf{q}}}, t)$ 8 // compute motion field drift and task score $\Upsilon'_t \leftarrow \Upsilon'_t(\mathbf{q}_t \mid \mathcal{T})$ (Eq. 9a) 10 $s_t \leftarrow \nabla \log p_t(\mathbf{q}_t \mid \mathcal{T})$ (Eq. 9b) 11 // train neural motion field and score function 12 $\widehat{\Upsilon}_t \leftarrow \Upsilon_{\theta}(\mathbf{q}_t, t), \quad \widehat{s}_t \leftarrow s_{\theta}(\mathbf{q}_t, t)$ 13 $\mathcal{L}(\theta) \leftarrow \|\widehat{\Upsilon}_t - \Upsilon'_t\|_2^2 + \lambda(t) \|\widehat{s}_t - s_t\|_2^2$ (Eq. 11) 14 $\theta \leftarrow \theta - \eta \nabla_{\theta} \mathcal{L}(\theta)$ 15

Input: $\pi_0 \coloneqq$ noise distributions, $\delta \coloneqq$ timestep $\mathcal{T} = [\mathbf{q}_0, \mathbf{q}_T] \coloneqq$ task (start & goal states)

16

23

24

return $\Upsilon_{\theta}, s_{\theta}$

 $t \leftarrow t + \delta$

return [q, q, q]

Output: $[\mathbf{q}, \dot{\mathbf{q}}, \ddot{\mathbf{q}}] \coloneqq \text{task-conditioned robot motion}$ 17 function generate_motion($\pi_0, \delta, \mathcal{T}$)

18 $|\mathbf{q}, \dot{\mathbf{q}}, \ddot{\mathbf{q}} = \varepsilon_{\mathbf{Q}}, \varepsilon_{\dot{\mathbf{Q}}}, \varepsilon_{\ddot{\mathbf{Q}}} \leftarrow \pi_0, \quad t \leftarrow 0$ 19 while $t \le 1$ do

20 $|s \leftarrow s_{\theta}(t, \mathbf{q}, \dot{\mathbf{q}}, \ddot{\mathbf{q}}, \mathcal{T})|$ 21 $|\Upsilon \leftarrow \Upsilon_{\theta}(t, \mathbf{q}, \dot{\mathbf{q}}, \ddot{\mathbf{q}}, \mathcal{T}) - \frac{1}{2} \sigma_t^2 s$ (Eq. 12)

22 $|[\mathbf{q}, \dot{\mathbf{q}}, \ddot{\mathbf{q}}] \leftarrow [\mathbf{q}, \dot{\mathbf{q}}, \ddot{\mathbf{q}}] + \Upsilon \cdot \delta$

flow-matching settings, the marginals, $p_t(\pi) = \mathcal{N}\left(\mu_{\pi}, \sigma_{\pi}^2\right)$, admit the following closed form with the Schrödinger bridges from π_0 to π_1 and a constant diffusion rate $\sigma \equiv \sigma_t$:

$$p_t(\pi) = \mathcal{N}\left(t\pi_1 + (1-t)\pi_0, \ \sigma^2 t(1-t)\right).$$
 (6)

From Eq. 5 and Eq. 6, the motion field ODE and the score function are thus expressed as:

$$\Upsilon'_t(\psi(\pi)) = \alpha(t)(\pi - \mu_\pi) + (\pi_1 - \pi_0),$$
 (7a)

$$\nabla \log p_t(\pi) = (\mu_{\pi} - \pi)/\sigma_{\pi}^2, \tag{7b}$$

where $\alpha(t)$ is a transport weighting term induced by the interpolants. Here, Eq. 7a and Eq. 7b provide the Schrödinger bridge-based motion field in unconditioned settings.

C. Task-Conditioned Motion Field with Schrödinger Bridges

Two important aspects of realizing task-conditioned robot motions are score-based functions and motion fields. The score-based function serves as a guided sampling mechanism post-contextualization. Meanwhile, the motion field refers to the generation of a trajectory given start and goal states.

Given the set of N distinct tasks $\mathcal{T} = \bigcup_{i=1}^{N} \mathcal{T}_i$, Eq. 6 with any task \mathcal{T} can be modeled as:

$$p_t(\pi \mid \mathcal{T}) = \mathcal{N}\left(t\pi_1^{\mathcal{T}} + (1-t)\pi_0^{\mathcal{T}}, \ \sigma_{\mathcal{T}}^2 t (1-t)\right), \quad (8)$$

with $\bigcup_{i=1}^N \pi^{\mathcal{T}_i} \subseteq \pi$, $\bigcup_{i=1}^N \pi_0^{\mathcal{T}_i} \subseteq \pi_0$, and $\bigcup_{i=1}^N \pi_1^{\mathcal{T}_i} \subseteq \pi_1$ representing the task-dependent intermediate, source, and expert motion distributions along the evolving probability flow $p_t(\pi \mid \mathcal{T})$, respectively. With Eq. 8, the motion field ODE (Eq. 7a) and score function (Eq. 7b) are then adjusted to reflect the task dependency as follows:

$$\Upsilon_{t}'\left(\psi\left(\pi\right)\mid\mathcal{T}\right) = \alpha(t)\left(\pi - \mu_{\pi}\tau\right) + \left(\pi_{0}^{\mathcal{T}} - \pi_{0}^{\mathcal{T}}\right), \quad (9a)$$

$$\nabla \log p_t \left(\pi \mid \mathcal{T} \right) = \left(\mu_{\pi^{\mathcal{T}}} - \pi^{\mathcal{T}} \right) / \sigma_{\pi^{\mathcal{T}}}^2. \tag{9b}$$

Eq. 9a exemplifies the incorporation of task-dependent variations in transport behavior while still being grounded with Schrödinger bridges. Meanwhile, Eq. 9b characterizes the score-based function that guides the trajectory generation in latent space to maximize task likelihood. To preserve high-order dynamics, we also incorporate time-dependent interpolants for path, velocity, and acceleration profiles, while training the motion field Υ_t [27]:

$$\mathbf{q}_t = (1 - t)\,\varepsilon_{\mathbf{q}} + t\,\mathbf{q}_1,\tag{10a}$$

$$\mathbf{q}_t = (1 - t^2) \,\varepsilon_{\mathbf{q}} + (t - t^2) \,\varepsilon_{\dot{\mathbf{q}}} + t^2 \,\mathbf{q}_1, \tag{10b}$$

$$\mathbf{q}_t = (1 - t^3) \,\varepsilon_{\mathbf{q}} + (t - t^3) \,\varepsilon_{\dot{\mathbf{q}}} + \frac{t^2 - t^3}{2} \,\varepsilon_{\ddot{\mathbf{q}}} + t^3 \,\mathbf{q}_1, \tag{10c}$$

where \mathbf{q}_t acts as the evolving probability flow of \mathbf{q} , while transporting it from $\varepsilon_{\mathbf{q}} \in \varepsilon_{\mathbf{Q}}$ to $\mathbf{q}_1 \in \mathbf{Q}$, and $\varepsilon_{\dot{\mathbf{q}}} \in \varepsilon_{\dot{\mathbf{Q}}}$ and $\varepsilon_{\dot{\mathbf{q}}} \in \varepsilon_{\dot{\mathbf{Q}}}$ denote the noise initializations for first- and second-order dynamics of \mathbf{q} along the intermediate distribution π .

To learn both the score-based function and the motion field simultaneously, we employ two U-Nets [49] corresponding to Eq. 9a and Eq. 9b that jointly learn contextualized evolving entropic flows p_t (π | \mathcal{T}) from $\pi_0^{\mathcal{T}}$ to $\pi_1^{\mathcal{T}}$. We train two neural SDEs to approximate (i) the motion field Υ_t and (ii) the score function $\nabla \log p_t(\cdot \mid \mathcal{T})$ through the combined loss of flow-matching and score-matching, thereby solving Eq. 2:

$$\mathcal{L}(\theta) = \|\Upsilon_{\theta} - \Upsilon_{t}^{'}\|_{2}^{2} + \lambda(t) \|s_{\theta} - \nabla \log p_{t}(\pi \mid \mathcal{T})\|_{2}^{2}, \quad (11)$$

where $\lambda(t)$ represents the scheduler, Υ_{θ} is the learned motion field, and s_{θ} is the learned score function. The motion field Υ_{θ} also learns the sub-fields for high-order dynamics via the learnable parameters $\theta = \{\theta_1, \theta_2, \theta_3\}$, as detailed in Eq. 10.

D. Inference of Task-Conditioned Motion Field

After training governed by Eq. 11, to infer the optimal task-conditioned motion field, we estimate the transport paths by updating the transport drift and the score function. The entropic flow follows the motion field ODE: $d\psi_t = \Upsilon_t'(\psi(\pi) \mid \mathcal{T}) dt$, which moves the samples $\pi^{\mathcal{T}}$ from $\pi_0^{\mathcal{T}}$ to $\pi_1^{\mathcal{T}}$. With k as the number of update steps in the time range from 0 to 1, the motion field with the score function that pushes noise samples π_0 toward high-likelihood expert motions while incorporating the task condition \mathcal{T} is:

$$\Upsilon_{t}^{(k+1)}\left(\psi\left(\pi\right)\mid\mathcal{T}\right) = \Upsilon_{\theta}^{(k)}\left(t,\psi\left(\pi\right)\mid\mathcal{T}\right) - \frac{1}{2}\sigma^{2}s_{\theta}\left(t,\pi\mid\mathcal{T}\right). \tag{12}$$

TABLE I: Quantitative comparisons of XFlowMP against other flow matching-based methods [16], [50], [51] in terms of maximum mean discrepancy (MMD), trajectory jerkiness (TJ), and energy consumption (EC). For all benchmarked methods, the lengths of generated trajectories are 256 in the RobotPointMass environment [27] and 1,000 in the LASA Handwriting dataset [52], respectively.

	Environment / Metric	RobotPointMass (L = 256)			LASA Handwriting (L = 1,000)		
Method	/ Metric	MMD (↓) (Eq. 13)	TJ (↓) (Eq. 14)	EC (\(\psi\) (Eq. 15)	MMD (↓) (Eq. 13)	TJ (↓) (Eq. 14)	EC (\(\psi\) (Eq. 15)
	Lipman et al. [16]	12590.54	101.58 ± 7.55	8695.78 ± 534.74	39.88	2507.17 ± 176.03	215263.84 ± 12407.40
	Tong et al. [50]	34.63	0.17 ± 0.10	15.93 ± 8.60	20.18	2.78 ± 1.73	231.40 ± 158.54
	Albergo et al. [51]	31.42	0.11 ± 0.06	9.83 ± 4.65	19.07	4.97 ± 4.39	432.17 ± 360.72
	XFlowMP (Ours)	14.52	$\textbf{0.07}\pm\textbf{0.04}$	5.91 ± 3.63	18.83	2.67 ± 1.31	157.43 ± 97.16
	vs. 2nd Best	+53.79 % ↑	+36.36% ↑	+39.88% ↑	+1.26 % ↑	+3.96 % ↑	+31.97% ↑

By applying k-step optimization, Eq. 12 is able to generate smooth, scalable, collision-free, dynamically-feasible, task-adaptive robot motions with high-order dynamics under contextualization. We outline our proposed method, as illustrated in Fig. 2 and described algorithmically in Alg. 1.

IV. EVALUATIONS & EXPERIMENTS

A. Evaluation Baselines & Questions

- 1) Datasets & Baselines: To assess XFlowMP's performance comprehensively, we evaluate our proposed method in terms of distributional discrepancy, trajectory jerkiness, and curves with least energy, on the RobotPointMass dataset [27], where expert motions are generated using VP-STO [53], and the LASA Handwriting dataset [52] with high-fidelity written character writings. The experimented baselines include three flow matching variants:
 - Lipman *et al.* [16]: A foundational work that aligns generated samples directly to targets through flows.
 - Tong et al. [50]: A variant that leverages the theory of optimal transport to compute exact displacement fields between source and target distributions.
 - Albergo *et al.* [51]: Another approach that introduces stochastic flows with trigonometric interpolants.
- 2) Evaluation Questions: All algorithms are benchmarked using the same network architecture, trained for 30 epochs on the NVIDIA RTX 4090 GPU with initialized noises randomly generated within the robot workspace. Our evaluations are to answer the following key questions:
 - **Q1:** How well do generated trajectories by X*FlowMP* match the expert trajectory distribution?
 - **Q2:** Are those generated trajectories smoother or jerkier compared to those generated by baseline methods?
 - Q3: Given the first two criteria, whether the generated trajectories by our proposed method follow paths of lower curve-energy compared to baseline methods?
 - Q4: Does Schrödinger-based approach yield better contextualization and scalability while generating collisionfree and dynamically-feasible motions?
 - **Q5:** Across the benchmarked algorithms, how do the generated motions compare to each other qualitatively?

B. Quantitative Results

1) Maximum Mean Discrepancy (MMD): First, to measure the distance between the generated and the learning

distributions in order to answer Q1, we use MMD [54] to evaluate their discrepancy in a reproducing kernel Hilbert space. Let $\mathcal{D}_{\text{gen}} = \{\mathbf{q}_i^{\text{gen}}\}_{i=1}^M$ be the set of M generated trajectories, the MMD score is defined as:

$$MMD\left(\mathcal{D}_{gen}, \mathcal{D}\right) = \frac{1}{M^2} \sum_{i,i'} k\left(\mathbf{q}_{i}^{gen}, \mathbf{q}_{i'}^{gen}\right)$$
$$-\frac{2}{MN} \sum_{i,j} k\left(\left(\mathbf{q}_{i}^{gen}, \mathbf{q}_{j}\right) + \frac{1}{N^2} \sum_{i,j'} k\left(\mathbf{q}_{j}, \mathbf{q}_{j'}\right), \quad (13)$$

where $k(\cdot, \cdot)$ represents the positive definite kernel.

In the RobotPointMass environment, XFlowMP achieves the lowest MMD of 14.52, outperforming prior flow matching variants, including Albergo et al. and Tong et al., as shown in Tab. I. Meanwhile, on the more challenging LASA Handwriting dataset, XFlowMP retains a lower MMD of 18.83, slightly below Albergo et al. and surpassing Tong et al.. Overall, these MMD scores demonstrate that XFlowMP is able to maintain distributional consistency with respect to expert motions for both short- and long-horizon planning.

2) Trajectory Jerkiness: Next, to quantify the jerkiness of the generated trajectory for $\mathbf{Q2}$, we compute the integrated squared acceleration along the trajectory. Along the planning horizon T, we calculate the trajectory jerkiness as:

$$TJ(\mathbf{q}) = \int_0^T \|\ddot{\mathbf{q}}(t)\|_2^2 dt, \tag{14}$$

Tab. I also shows that XFlowMP consistently produces the lowest values on both datasets. In the RobotPointMass environment, our method attains 0.07 ± 0.04 , a substantial improvement over Albergo et~al. and Tong et~al.. On the LASA Handwriting dataset, XFlowMP again achieves the best performance with 2.67 ± 1.31 , improving upon Tong $et~al.~(2.78 \pm 1.73)$ and Albergo $et~al.~(4.97 \pm 4.39)$. Through these jerkiness scores, we confirm that our method generates smoother and physically-feasible motions.

3) Energy Consumption: To answer Q3, we assess the efficiency of the generated trajectory by measuring its total kinetic energy along the horizon T, as follows:

$$EC(\mathbf{q}) = \int_0^T ||\dot{\mathbf{q}}(t)||_2^2 dt, \tag{15}$$

Given the correctness of the first two criteria, XFlowMP also achieves the lowest energy consumption among the benchmarked methods, as depicted in Tab. I. In the RobotPointMass environment, our method retains the

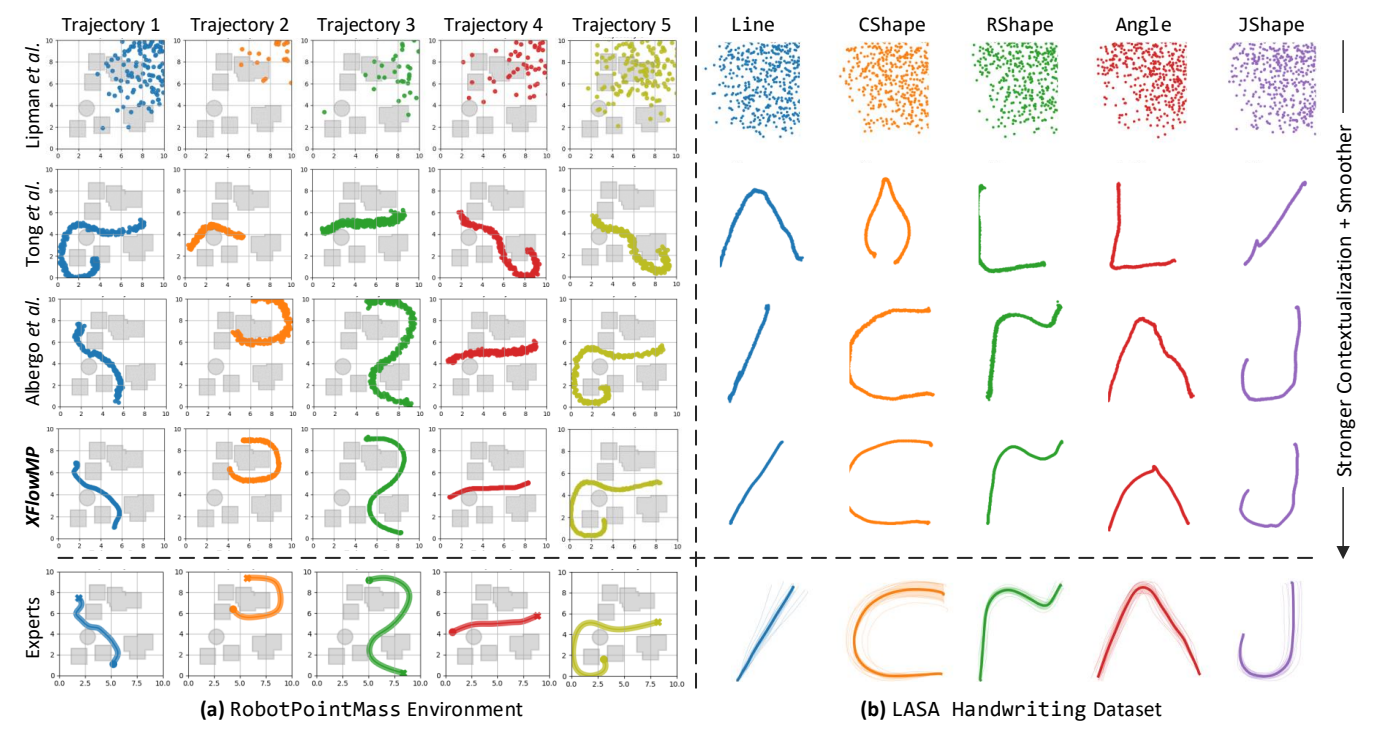


Fig. 3: Qualitative Comparisons of Trajectories Generated by Baselines and XFlowMP: (a) In the RobotPointMass environment, XFlowMP produces smooth, collision-free paths that closely follow expert demonstrations, while baselines often yield discontinuous or collision-prone trajectories. (b) On the LASA Handwriting dataset, XFlowMP captures the structure of complex patterns, aligning well with expert motions. In contrast, baseline methods tend to generate incorrect/distorted shapes or fail to preserve curvature. Generally, XFlowMP exhibits a strong ability to contextualize while producing smooth, collision-free, and expert-like trajectories.

TABLE II: Planning feasibility for both short- and long-horizon motions among all flow matching-based motion planning baselines.
✓ denotes success of and ✗ denotes failure to reach targets. Also, the number of successful task contextualizations is reported.

Length	RobotPointMass (L = 256)	LASA Handwriting (L = 1,000)
Lipman et al. [16]	0/10 (X)	0/10 (X)
Tong et al. [50]	5/10 (X)	7/10 (X)
Albergo et al. [51]	10/10 (✓)	10/10 (🗸)
XFlowMP (Ours)	10/10 (🗸)	10/10 (🗸)

energy consumption of 5.91 ± 3.63 , which is substantially lower than Albergo et~al. and Tong et~al. Similarly, on LASA Handwriting dataset, XFlowMP produces the most energy-efficient trajectories with 157.43 ± 97.16 , much lower than Tong et~al. and Albergo et~al., further indicating that XFlowMP generates trajectories that are not only smooth but also energy efficient compared to other baselines.

4) Summary: Taken together, these results showcase that XFlowMP yields trajectories that achieve superior distributional alignment, smoothness, and energy efficiency compared to state-of-the-art flow matching baselines. Notably, our method demonstrates effective scalability across a range of horizons, from short to long, showing strong adaptability to the requirements of trajectory resolutions.

C. Planning Feasibility & Inference time

1) Planning Feasibility: To quantitatively answer Q4, we evaluate planning feasibility based on the number of successful planned paths over the tested paths, as shown in

TABLE III: Benchmarking the planning/inference time (in *seconds*) for both short- and long-horizon motions among baselines.

Time	Planning Time (L = 256)	Planning Time (L = 1,000)
Lipman et al. [16]	_	_
Tong et al. [50]	0.1911 ± 0.0240	0.1973 ± 0.0364
Albergo et al. [51]	0.2477 ± 0.0310	0.2859 ± 0.0817
XFlowMP (Ours)	0.1687 ± 0.0393	0.2577 ± 0.1255
vs. 2nd Best	+11.72 % ↑	-30.61% ↓

Tab. II. The results of feasibility show that both XFlowMP and Albergo et al. reach perfect success rates, producing collision-free and goal-reaching trajectories in both short-and long-horizon tasks. Lipman et al. fails in every test case, while Tong et al. only manages partial success, with 5/10 valid trajectories in short-horizon and 7/10 in long-horizon planning. XFlowMP demonstrates strong reliability across different planning horizons and maintains consistent performance compared to the state-of-the-art baselines, which also yields that the usage of Schrödinger bridges is more suitable for task-adaptive planning conditions and requirements compared to other methods.

2) Inference Time: Table III benchmarks the inference time of XFlowMP against prior flow matching-based methods for both short- and long-horizon motion generation. While not the overall fastest, XFlowMP achieves the inference times of 0.1689 and 0.2577 seconds on the RobotPointMass and LASA Handwriting datasets, respectively. Notably, XFlowMP yields the plan-



Fig. 4: Real-Robot Demonstration: Using X*FlowMP*, the Kinova Gen3 manipulator is able to generate smooth, collision-free, and dynamically-feasible motions to reach the LEGO block on the shelf, given the positions of the robot and the target object as the task.

ning/inference time of about 11.72% faster than Albergo *et al.*, which achieves second-best performance quantitatively in RobotPointMass, and about 0.06 seconds slower than Tong *et al.* that retains second-best performance quantitatively in LASA Handwriting dataset. Together with Table I, where XFlowMP demonstrates its gains in distributional alignment, generated trajectory quality, and energy efficiency, we acknowledge that these only lead to a modest increase in computational cost for long-horizon planning.

D. Qualitative Results & Limitations

1) Qualitative Results: As shown in Fig. 3, for answering Q5, XFlowMP generates smooth and collision-free trajectories that follow expert demonstrations in the RobotPointMass environment (Fig. 3a). Meanwhile, other methods often encounter discontinuous and obstacle-colliding motions. In Fig. 3b, on the LASA Handwriting dataset, our method accurately captures the geometric structure of motion patterns, as illustrated in Line, CShape, RShape, Angle, and JShape, producing motions that remain well-aligned with expert references. In contrast, other approaches experience shape distortion and fail to maintain smooth curvature. Overall, we show that XFlowMP is able to demonstrate its strong contextualization and good quality across short- and long-horizon planning, producing qualitatively superior motions compared to all baseline methods.

2) Limitations: While our method scales well and produces smooth, task-adaptive motions, we find that its effectiveness largely depends on the task-agnosticity of the expert demonstrations. For example, failure cases occur when multiple experts propose outrageously different motions for a single task, resulting in collapsed learning distributions, even with a well-trained task-conditioned motion field.

E. Real-Robot Experiments

We validate the feasibility of XFlowMP on a real-robot system using the Kinova Gen3 manipulator. In this experiment, the task is defined by the positions of the robot and the target LEGO block placed on a shelf. XFlowMP is trained on 10 expert demonstrations per planning mode, capturing smooth and dynamically-feasible trajectories under varying start—goal configurations. After training, the learned motion field is then deployed on the Kinova Gen3, connected to an Intel Core i9-14900 CPU and an NVIDIA RTX 4080S GPU. The robot is then able to generate collision-free motions to reach the LEGO block from different initial poses, given that the position of the LEGO block is known. As shown in Fig. 4, the robot successfully executes the generated trajectory to

reach the LEGO block while maintaining the smoothness and collision-free nature of expert demonstrations. Our demonstration videos are available in the supplementary materials.

V. Conclusions

This paper presents XFlowMP, a task-conditioned generative motion planner that models trajectories as entropic flows via Schrödinger bridges with score-based motion fields. Our method is able to generate smooth, collision-free, and dynamically feasible trajectories with high-order dynamics under environmental constraints through conditioning on start-goal configurations, enabling integration of task context into low-level motion generation. Through evaluations on the RobotPointMass and LASA Handwriting benchmarks, we show that XFlowMP achieves lower MMD, smoother motions, and lower energy consumption, while reducing short-horizon planning time and guaranteeing planning feasibility across both short- and long-horizon motions. Our real-world experiments on the Kinova Gen3 manipulator further confirm that the framework can reliably generate feasible trajectories, highlighting its potential for scalable, adaptable motion planning in real-world settings.

REFERENCES

- L. E. Kavraki, P. Svestka, J.-C. Latombe, and M. H. Overmars, "Probabilistic roadmaps for path planning in high-dimensional configuration spaces," *IEEE transactions on Robotics and Automation*, vol. 12, no. 4, pp. 566–580, 2002.
- [2] S. M. LaValle and J. J. Kuffner, "Rapidly-exploring random trees: Progress and prospects: Steven m. lavalle, iowa state university, a james j. kuffner, jr., university of tokyo, tokyo, japan," Algorithmic and computational robotics, pp. 303–307, 2001.
- [3] N. Ratliff, M. Zucker, J. A. Bagnell, and S. Srinivasa, "Chomp: Gradient optimization techniques for efficient motion planning," in 2009 IEEE international conference on robotics and automation. IEEE, 2009, pp. 489–494.
- [4] J. Schulman, J. Ho, A. X. Lee, I. Awwal, H. Bradlow, and P. Abbeel, "Finding locally optimal, collision-free trajectories with sequential convex optimization." in *Robotics: science and systems*, vol. 9, no. 1. Berlin, Germany, 2013, pp. 1–10.
- [5] G. Papadopoulos, H. Kurniawati, and N. M. Patrikalakis, "Analysis of asymptotically optimal sampling-based motion planning algorithms for lipschitz continuous dynamical systems," arXiv preprint arXiv:1405.2872, 2014.
- [6] E. Beeching, J. Dibangoye, O. Simonin, and C. Wolf, "Learning to plan with uncertain topological maps," in *European Conference on Computer Vision*. Springer, 2020, pp. 473–490.
- [7] V. R. Somnath, M. Pariset, Y.-P. Hsieh, M. R. Martinez, A. Krause, and C. Bunne, "Aligned diffusion schrödinger bridges," in *Uncertainty in Artificial Intelligence*. PMLR, 2023, pp. 1985–1995.
- [8] A. Tong, N. Malkin, K. Fatras, L. Atanackovic, Y. Zhang, G. Huguet, G. Wolf, and Y. Bengio, "Simulation-free schr\" odinger bridges via score and flow matching," arXiv preprint arXiv:2307.03672, 2023.

- [9] V. De Bortoli, J. Thornton, J. Heng, and A. Doucet, "Diffusion schrödinger bridge with applications to score-based generative modeling," *Advances in neural information processing systems*, vol. 34, pp. 17 695–17 709, 2021.
- [10] Y. Shi, V. De Bortoli, A. Campbell, and A. Doucet, "Diffusion schrödinger bridge matching," *Advances in Neural Information Pro*cessing Systems, vol. 36, pp. 62 183–62 223, 2023.
- [11] Q. P. Pham, K. T. Nguyen, N. H. Doan, C. A. Pham, Q. Sun, W. Qi, K. Inui, and D. Song, "Smallplan: Leverage small language models for sequential path planning with simulation-powered, Ilmguided distillation," arXiv preprint arXiv:2505.00831, 2025.
- [12] Z. Chen, G. He, K. Zheng, X. Tan, and J. Zhu, "Schrodinger bridges beat diffusion models on text-to-speech synthesis," arXiv preprint arXiv:2312.03491, 2023.
- [13] D. P. Kingma and M. Welling, "Auto-encoding variational bayes," arXiv preprint arXiv:1312.6114, 2013.
- [14] K. Sohn, H. Lee, and X. Yan, "Learning structured output representation using deep conditional generative models," *Advances in neural information processing systems*, vol. 28, 2015.
- [15] D. Rezende and S. Mohamed, "Variational inference with normalizing flows," in *International conference on machine learning*. PMLR, 2015, pp. 1530–1538.
- [16] Y. Lipman, R. T. Chen, H. Ben-Hamu et al., "Flow matching for generative modeling," arXiv preprint arXiv:2210.02747, 2022.
- [17] J. Ho, A. Jain, and P. Abbeel, "Denoising diffusion probabilistic models," *Advances in neural information processing systems*, vol. 33, pp. 6840–6851, 2020.
- [18] Y. Song, J. Sohl-Dickstein, D. P. Kingma, A. Kumar, S. Ermon, and B. Poole, "Score-based generative modeling through stochastic differential equations," arXiv preprint arXiv:2011.13456, 2020.
- [19] P. Dhariwal and A. Nichol, "Diffusion models beat gans on image synthesis," *Advances in neural information processing systems*, vol. 34, pp. 8780–8794, 2021.
- [20] R. Rombach, A. Blattmann, D. Lorenz, P. Esser, and B. Ommer, "High-resolution image synthesis with latent diffusion models," in Proceedings of the IEEE/CVF conference on computer vision and pattern recognition, 2022, pp. 10684–10695.
- [21] M. Janner, Y. Du, J. B. Tenenbaum, and S. Levine, "Planning with diffusion for flexible behavior synthesis," arXiv preprint arXiv:2205.09991, 2022.
- [22] C. Chi, Z. Xu, S. Feng, E. Cousineau, Y. Du, B. Burchfiel, R. Tedrake, and S. Song, "Diffusion policy: Visuomotor policy learning via action diffusion," *The International Journal of Robotics Research*, p. 02783649241273668, 2023.
- [23] A. Tong, J. Huang, G. Wolf, D. Van Dijk, and S. Krishnaswamy, "Trajectorynet: A dynamic optimal transport network for modeling cellular dynamics," in *International conference on machine learning*. PMLR, 2020, pp. 9526–9536.
- [24] Y. Rubanova, R. T. Chen, and D. K. Duvenaud, "Latent ordinary differential equations for irregularly-sampled time series," Advances in neural information processing systems, vol. 32, 2019.
- [25] C. Lynch, M. Khansari, T. Xiao, V. Kumar, J. Tompson, S. Levine, and P. Sermanet, "Learning latent plans from play," in *Conference on robot learning*. Pmlr, 2020, pp. 1113–1132.
- [26] E. Jang, A. Irpan, M. Khansari, D. Kappler, F. Ebert, C. Lynch, S. Levine, and C. Finn, "Bc-z: Zero-shot task generalization with robotic imitation learning," in *Conference on Robot Learning*. PMLR, 2022, pp. 991–1002.
- [27] K. Nguyen, A. T. Le, T. Pham, M. Huber, J. Peters, and M. N. Vu, "Flowmp: Learning motion fields for robot planning with conditional flow matching," arXiv preprint arXiv:2503.06135, 2025.
- [28] F. Vargas, W. Grathwohl, and A. Doucet, "Denoising diffusion samplers," arXiv preprint arXiv:2302.13834, 2023.
- [29] J. Wen, Y. Zhuang, and J. Deng, "Edm: a enhanced diffusion models for image restoration in complex scenes," *The Visual Computer*, vol. 41, no. 4, pp. 2511–2527, 2025.
- [30] T. Xu, L. K. Wenliang, M. Munn, and B. Acciaio, "Cot-gan: Generating sequential data via causal optimal transport," *Advances in neural* information processing systems, vol. 33, pp. 8798–8809, 2020.
- [31] Z. Shen, J. Feydy, P. Liu, A. H. Curiale, R. San Jose Estepar, R. San Jose Estepar, and M. Niethammer, "Accurate point cloud registration with robust optimal transport," *Advances in Neural Information Processing Systems*, vol. 34, pp. 5373–5389, 2021.
- [32] G. Huguet, D. S. Magruder, A. Tong, O. Fasina, M. Kuchroo, G. Wolf, and S. Krishnaswamy, "Manifold interpolating optimal-transport flows

- for trajectory inference," Advances in neural information processing systems, vol. 35, pp. 29705–29718, 2022.
- [33] J. Brehmer, J. Bose, P. De Haan, and T. S. Cohen, "Edgi: Equivariant diffusion for planning with embodied agents," *Advances in Neural Information Processing Systems*, vol. 36, pp. 63818–63834, 2023.
- [34] P. Kidger, J. Morrill, J. Foster, and T. Lyons, "Neural controlled differential equations for irregular time series," *Advances in neural* information processing systems, vol. 33, pp. 6696–6707, 2020.
- [35] J. Ho and T. Salimans, "Classifier-free diffusion guidance," arXiv preprint arXiv:2207.12598, 2022.
- [36] C. Saharia, W. Chan, S. Saxena, L. Li, J. Whang, E. L. Denton, K. Ghasemipour, R. Gontijo Lopes, B. Karagol Ayan, T. Salimans et al., "Photorealistic text-to-image diffusion models with deep language understanding," Advances in neural information processing systems, vol. 35, pp. 36479–36494, 2022.
- [37] D. J. Zhang, J. Z. Wu, J.-W. Liu, R. Zhao, L. Ran, Y. Gu, D. Gao, and M. Z. Shou, "Show-1: Marrying pixel and latent diffusion models for text-to-video generation," *International Journal of Computer Vision*, vol. 133, no. 4, pp. 1879–1893, 2025.
- [38] U. Singer, A. Polyak, T. Hayes, X. Yin, J. An, S. Zhang, Q. Hu, H. Yang, O. Ashual et al., "Make-a-video: Text-to-video generation without text-video data," arXiv preprint arXiv:2209.14792, 2022.
- [39] Y. Jiang, A. Gupta, Z. Zhang, G. Wang, Y. Dou, Y. Chen, L. Fei-Fei, A. Anandkumar, Y. Zhu, and L. Fan, "Vima: General robot manipulation with multimodal prompts," arXiv preprint arXiv:2210.03094, vol. 2, no. 3, p. 6, 2022.
- [40] H. Huang, X. Chen, Y. Chen, H. Li, X. Han, Z. Wang, T. Wang, J. Pang, and Z. Zhao, "Roboground: Robotic manipulation with grounded vision-language priors," in *Proceedings of the Computer Vision and Pattern Recognition Conference*, 2025, pp. 22540–22550.
- [41] A. Zeng, P. Florence, J. Tompson, S. Welker, J. Chien, M. Attarian, T. Armstrong, I. Krasin, D. Duong, V. Sindhwani et al., "Transporter networks: Rearranging the visual world for robotic manipulation," in Conference on Robot Learning. PMLR, 2021, pp. 726–747.
- [42] S. R. Sahoo, S. P. Sahoo, A. Jena, and K. Pati, "Optimal control on schrödinger lie group and the behaviour of the dynamics," *IMA Journal* of Mathematical Control and Information, pp. 213–229, 2018.
- [43] K. Bakshi, D. D. Fan, and E. A. Theodorou, "Schrödinger approach to optimal control of large-size populations," *IEEE Transactions on Automatic Control*, vol. 66, no. 5, pp. 2372–2378, 2020.
- [44] K. F. Caluya and A. Halder, "Reflected schrödinger bridge: Density control with path constraints," in 2021 American Control Conference (ACC). IEEE, 2021, pp. 1137–1142.
- [45] A. Eldesoukey and T. T. Georgiou, "Schrödinger's control and estimation paradigm with spatio-temporal distributions on graphs," *IEEE Transactions on Automatic Control*, 2024.
- [46] M. Mirrahimi, P. Rouchon, and G. Turinici, "Lyapunov control of bilinear schrödinger equations," *Automatica*, vol. 41, no. 11, pp. 1987– 1994, 2005.
- [47] A. D. Fokker, "Die mittlere energie rotierender elektrischer dipole im strahlungsfeld," Annalen der Physik, pp. 810–820, 1914.
- [48] V. Planck, "Über einen satz der statistischen dynamik und seine erweiterung in der quantentheorie," Sitzungberichte der, 1917.
- [49] O. Ronneberger, P. Fischer, and T. Brox, "U-net: Convolutional networks for biomedical image segmentation," in *Medical image* computing and computer-assisted intervention–MICCAI 2015: 18th international conference, Munich, Germany, October 5-9, 2015, proceedings, part III 18. Springer, 2015, pp. 234–241.
- [50] A. Tong, K. Fatras, N. Malkin, G. Huguet, Y. Zhang, J. Rector-Brooks, G. Wolf, and Y. Bengio, "Improving and generalizing flow-based generative models with minibatch optimal transport," arXiv preprint arXiv:2302.00482, 2023.
- [51] M. S. Albergo, N. M. Boffi, and E. Vanden-Eijnden, "Stochastic interpolants: A unifying framework for flows and diffusions," arXiv preprint arXiv:2303.08797, 2023.
- [52] A. Lemme, Y. Meirovitch, M. Khansari-Zadeh, T. Flash, A. Billard, and J. J. Steil, "Open-source benchmarking for learned reaching motion generation in robotics," *Paladyn, Journal of Behavioral Robotics*, vol. 6, no. 1, p. 000010151520150002, 2015.
- [53] J. Jankowski, L. Brudermüller, N. Hawes, and S. Calinon, "Vp-sto: Via-point-based stochastic trajectory optimization for reactive robot behavior," arXiv preprint arXiv:2210.04067, 2022.
- [54] A. Gretton, K. M. Borgwardt, M. J. Rasch, B. Schölkopf, and A. Smola, "A kernel two-sample test," *The journal of machine learning research*, vol. 13, no. 1, pp. 723–773, 2012.